CrossMark

Improvement of magnetic properties for V-substituted Fe$_{73.5}$Si$_{13.5}$B$_9$Cu$_1$Nb$_{3-x}$V$_x$ nanocrystalline alloys

Yabin Han[1] · Ran Wei[1] · Zichao Li[1] · Fushan Li[1] · Anding Wang[2] · Chuntao Chang[2] · Xinmin Wang[2]

Abstract The effects of V element on microstructural evolution and soft magnetic properties of Fe$_{73.5}$Si$_{13.5}$B$_9$Cu$_1$Nb$_{3-x}$V$_x$ (x = 0, 0.5,1, 1.5 and 2, at.%) nanocrystalline alloys annealed at one-step and two-step state were investigated. As a result of an adequate addition of V, the microstructure and soft magnetic properties of the nanocrystalline alloys have greatly changed. The alloys with higher V content are prone to form large grain size nanocomposite structure with better thermal stability but slightly worsen soft magnetic properties. However, the strategy of two-step annealing technique effectively refines grain and thereby improves the soft magnetic properties of the alloys. The nanocrystalline alloy with V = 1.5 after two-step annealing exhibits combined excellent soft magnetic properties, including a lower coercivity (H_c= 0.89 A/m), enhanced saturation magnetization (B_s over 1.3 T), high effective permeability? μ_e = 26,400 at 1 kHz) and low core loss. The work shows that adopting a preheating procedure before the primary nanocrystallization stage, viz. to use two-step annealing technique instead of the routinely used one-step nanocrystallization stage,is an effective solution to the disadvantage of the decrease of Nb.

✉ Fushan Li
   fsli@zzu.edu.cn

   Yabin Han
   elijahan1991@163.com

   Ran Wei
   weiranmse@zzu.edu.cn

   Zichao Li
   lizichao@nimte.ac.cn

   Anding Wang
   anding@nimte.ac.cn

   Chuntao Chang
   ctchang@nimte.ac.cn

   Xinmin Wang
   wangxm@nimte.ac.cn

[1] School of Materials Science and Engineering, Zhengzhou University, Zhengzhou 450001, China

[2] Key Laboratory of Magnetic Materials and Devices, Ningbo Institute of Materials Technology and Engineering, Chinese Academy of Sciences, Ningbo, Zhejiang 315201, China

1 Introduction

Since the development of FeSiBNbCu (Finemet) nanocrystalline alloys were found in 1988 [1], Fe-based soft magnetic nanocrystalline materials with anticipated excellent magnetic properties have attracted extensive interest. Compared with their crystal counterparts, high μ_e, moderate B_s, low H_c, and low core loss of nanocrystalline make them competent for the achievement of high efficiency, quietness and miniaturization in electromagnetic devices, e.g. transformers, sensors and inductors [1–8].

Soft magnetic nanocrystalline alloys are mostly fabricated from the amorphous alloys with partially crystallized precursors, resulting in a structure of ferromagnetic nanocrystals surrounded by a residual ferromagnetic amorphous matrix. The conventional nanocrystalline alloys contain some nonmagnetic metal elements, such as Nb, Zr, Mo, etc. that are regularly used to exert a suppression of the overgrowth of α-Fe crystalline phase and the precipitation of compounds such as tetragonal-Fe$_2$B and Fe$_3$B. This favours the formation of single α-Fe nanocrystalline phase upon primary crystallization, hence promoting the magnetic softness of the alloys [9, 10]. However, these added elements also result in the lower B_s and increase the costs of these alloys, for instance, the Fe$_{73.5}$Si$_{13.5}$B$_9$Cu$_1$Nb$_3$ alloy

has a rather low B_s of 1.23 T, and the cost of Nb element accounts for 90% of the total raw material cost [11, 12]. Therefore, researchers have intentionally investigated the effects of the substitution of low-cost Cr, V, Ta, etc. for nonmagnetic element Nb on the soft magnetic properties of these alloys. However, as a tradeoff of the lower cost than that of conventional Fe-based nanocrystalline alloys, the new alloy system suffers the disadvantage of larger structural correlation length (grain sizes) arising from the decrease of Nb, which have an uninviting effect on their magnetic softness, such as relatively high H_c of more than 2 A/m and low effective μ_e [11–14].

For the alloys, previous studies validate that preheating the samples at the optimal low temperature of 400 °C can prompt the Cu atoms to sufficiently gather to high density, increasing the nucleation sites during the initial stage of crystallization, which is an important approach to decrease α-Fe grain size [15, 16]. Hence, as a result of pretreating previous to the primary nanocrystallization stage, α-Fe crystals tend to form the structure of higher grain density, finer grain size and more uniform distribution, which are favorable for the soft magnetic properties [17, 18]. Accordingly, as our previous work [19], an alternative solution to the disadvantage of the decrease of Nb is adopting a pretreatment procedure before the primary nanocrystallization stage, viz. to use two-step annealing technique instead of the routinely used one-step nanocrystallization technique.

In this work, with the aim of lessening the unfavorable effect caused by decreasing the Nb content in the conventional nanocrystalline alloys, the FeSiBNbCu nanocrystalline alloy was selected as precursor alloy to systematically investigate the effects of V content on the structure, magnetic properties, thermal stability and magnetic domains of $Fe_{73.5}Si_{13.5}B_9Cu_1Nb_{3-x}V_x$ (x = 0, 0.5, 1, 1.5 and 2) nanocrystalline alloys. Further, in order to refine grain and optimize structure to reduce the deterioration of magnetic softness as partially substituting V for Nb, we implemented a two-step annealing technique for nanocrystallization of the selected alloys and researched its effect on the magnetic properties.

2 Experimental

Multicomponent alloy ingots with nominal percentage compositions of $Fe_{73.5}Si_{13.5}B_9Cu_1Nb_{3-x}V_x$ (x = 0, 0.5, 1, 1.5 and 2) were premelted by induction-melting mixtures of pure Fe (99.99 mass%), Cu (99.99 mass%), crystalline Si (99.99 mass%), and pre-alloyed Fe-B, Fe-Nb and Fe-V ingots under a high-purity argon atmosphere. Amorphous ribbons that are approximately 25 μm thick and 1 mm wide were fabricated by melt-spinning method with a wheel velocity of 40 m/s,which was much higher than the critical

cooling rate for single-amorphous phase formation. The structural characterization was examined by X-ray diffraction (XRD) with Cu–Kα radiation. Thermal stability associated with the initial temperature (T_x) and peak temperature (T_p) of crystallization for the as-quenched ribbons were measured by differential scanning calorimetry (DSC Netzsch 404 C) at a heating rate of 0.67 °C/s under high purity argon flow. The as-quenched ribbons were isothermally pretreated at 400 °C then annealed at high temperature ranging from 530 to 570 °C for 1h, respectively, under a vacuum followed by air-cooling to room temperature. The B_s was measured using a vibrating sample magnetometer (VSM, Lake Shore 7410) under a maximum applied field of 800 kA/m. The H_c was measured using a DC *B-H* loop tracer (RIKEN BHS-40) in a maximum applied field of 800 A/m. The μ_e at the frequency of 1 kHz was measured using a vector impedance analyzer (Agilent 4294 A) in a field of 1 A/m. The core loss of ribbons was measured with an AC *B-H* loop tracer at the frequency from 50 to 1000 Hz under induction 0.9 T. The magnetic domains in the unpolished ribbons have been imaged using an optical wide-field polarization microscope, applying the longitudinal magneto-optical Kerr effect. All images were obtained by subtracting the non-magnetic background. The longitudinal Kerr sensitivity was transverse to the ribbon edge along the microscope plane. As the magnetic properties are relative to the sample sizes, in the interest of clarifying the intrinsic soft magnetic properties of this alloy system, ribbon samples with similar size mentioned above were used for measurement. All measurements were performed at room temperature.

3 Results and discussion

The structure of the as-quenched ribbons used for thermal and magnetic tests were examined by XRD. Figure 1 shows the XRD results of as-quenched $Fe_{73.5}Si_{13.5}B_9Cu_1Nb_{3-x}V_x$ (x = 0, 0.5, 1, 1.5 and 2) alloy ribbons. All the XRD patterns of the as-quenched ribbons consist only of a broad peak and no peaks corresponding to crystalline phase, implying that these alloys are composed of a full amorphous phase.

To investigate the crystallization process, DSC measurements were performed. Figure 2 shows the DSC curves of the as-quenched alloys. All the curves have two distinct exothermic peaks, which demonstrates that the crystallization stages include two stages. The crystallization exothermic stages further confirm the amorphous structure of the alloys. With the addition of V element, the first crystallization T_{x1} decreases and the second onset temperature T_{x2} shows a same tendency, and the temperature interval ΔT_x (=$T_{x2}-T_{x1}$) first enlarges and then decreases. In
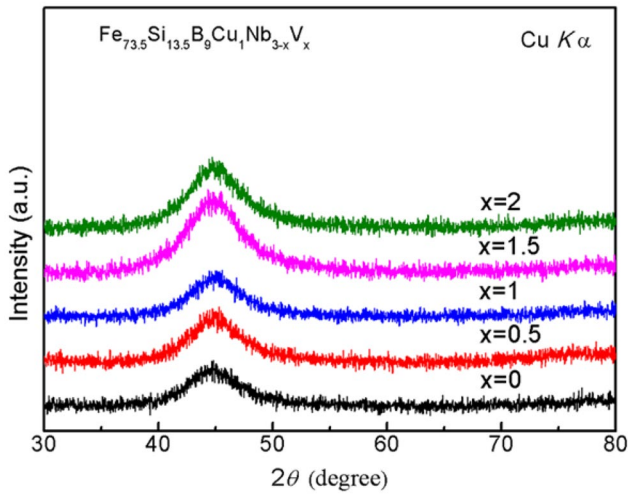
Fig. 1 XRD patterns of as-quenched $Fe_{73.5}Si_{13.5}B_9Cu_1Nb_{3-x}V_x$ ($x = 0$, 0.5, 1, 1.5 and 2) ribbons
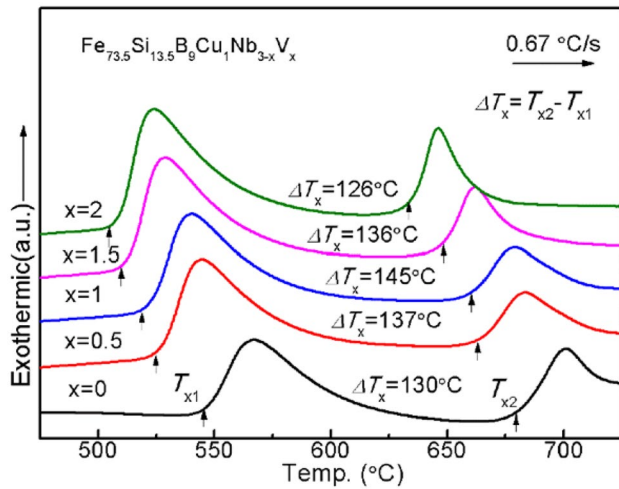
Fig. 2 DSC curves of the as-quenched $Fe_{73.5}Si_{13.5}B_9Cu_1Nb_{3-x}V_x$ ($x = 0$, 0.5, 1, 1.5 and 2) alloy ribbons at a heating rate of 0.67 °C/s

consequence, the maximum ΔT_x value reaches 145 °C for $Fe_{73.5}Si_{13.5}B_9Cu_1Nb_2V_1$ amorphous alloy. This indicates that adequate addition of V favors the precipitation of α-Fe and inhibits the precipitation of other compounds. Consequently, the adequate addition of V favors enlarging ΔT_x and thus enhancing the thermal stability of compounds relative to α-Fe phase precipitating from amorphous matrix. In addition, an amorphous precursor with a large ΔT_x can prompts the formation of α-Fe nanocrystalline and suppresses the precipitation of Fe_3B or Fe_2B non-ferromagnetic phases, which is favorable to achieve good soft magnetic properties.

For the as-quenched $Fe_{73.5}Si_{13.5}B_9Cu_1Nb_{3-x}V_x$ (x = 0, 0.5, 1, 1.5 and 2) alloys annealed by different technique,

the V content and temperature dependences of H_c are shown in Fig. 3. The H_c remains basically unchanged with the addition of V until V content reaches 1.5 at% when annealed through one-step technique, as shown in Fig. 3a. Upon the addition of V exceeding 1.5 at%, the H_c quickly increases along with the addition of V. Additionally, for the same V content, the higher annealing temperature lead to the higher H_c. Especially when V content surpasses the threshold value (x = 1.5), the discrepancy in the increase of H_c caused by rise in annealing temperature widens considerably. The results indicate that lower annealing temperature in favors of lower H_c and the alloys still have the characteristic of low H_c provided that the amount of Nb substituted by low-cost V which is no more than the half of its initial content. Furthermore, a preheating procedure before nanocrystallization stage was purposely added to remedy the disadvantage resulted from the decrease of Nb. By means of isothermally pretreatment at 400 °C for 1 h then annealing at high temperatures of 530 °C for 1h, namely a two-step annealing
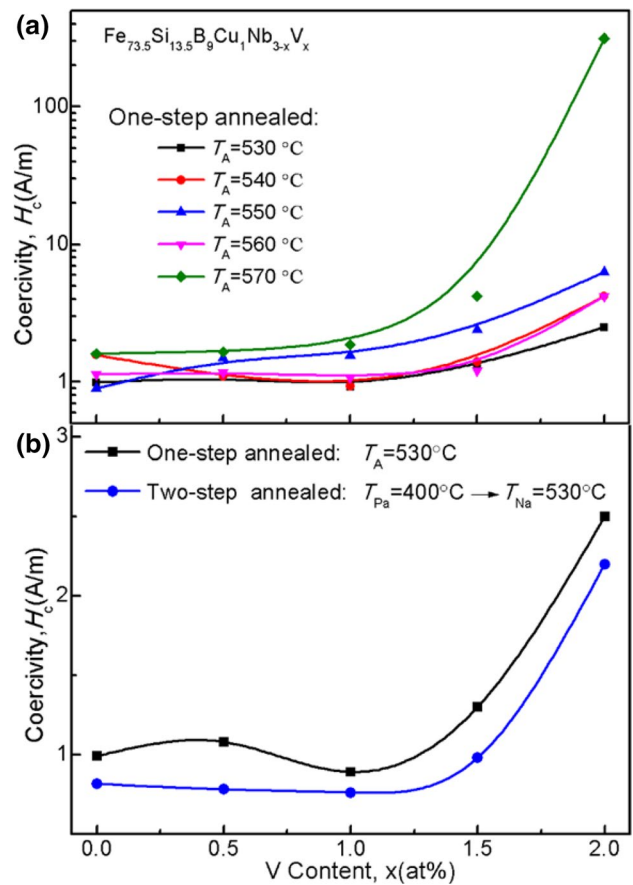

Fig. 3 Changes of H_c for the as-quenched $Fe_{73.5}Si_{13.5}B_9Cu_1Nb_{3-x}V_x$ ($x = 0$, 0.5, 1, 1.5 and 2) ribbons as a function of V content at one-step annealing (**a**) and two different annealing stages of optimized temperature for 1h (**b**), respectively

technique, the H_c manifestly decreases at each composition point of the alloys as compared with that by corresponding only one-step annealing stage at 530 °C for 1 h, as shown in Fig. 3b. According to the random anisotropy model [20], the change of H_c can be attributed to the variation of microstructure with applied pretreatment.

The dependence of effective permeability on frequency under an applied field at intensity of 1 A/m for the $Fe_{73.5}Si_{13.5}B_9Cu_1Nb_{3-x}V_x$ (x = 0, 0.5, 1, 1.5 and 2) nanocrystalline ribbons obtained by one-step annealing technique is shown in Fig. 4. The partial substitution of V for Nb results in a decrease of μ_e from 27,500 to 23,500 under the applied field at a frequency of 1 kHz. Moreover, the addition of V is very effective in enhancing the stability of μ_e against increase in frequency. Especially, the μ_e of alloys with V contents of x = 1.5 and 2 not only have as high as 26,100 and 26,000 at 1 kHz but also exhibit the highest stability against the increase of frequency. Specifically, the μ_e keep values as high as 25,000 and 24,000 when frequency increases to 10 kHz for the contained V alloys of 1.5 and 2 at%, respectively. In addition, adding V element also can improve cut-off frequency from 38 kHz to 52 kHz. As a result, even until at the cut-off frequency, the values of μ_e keep high values of 20,500 and 20,000 for the two alloys, respectively.

Figure 5 shows the dependence of μ_e on frequency for the $Fe_{73.5}Si_{13.5}B_9Cu_1Nb_{3-x}V_x$ (x = 0, 0.5, 1, 1.5 and 2) nanocrystalline alloys annealed by two-step technique. Compared with one-step annealing technique, the soft magnetic properties of the alloys are obviously improved. Under the applied field at a frequency of 1 kHz, the value of μ_e for the V-free alloy remains unchanged at 27,500, while those of μ_e for both of the alloys with V content
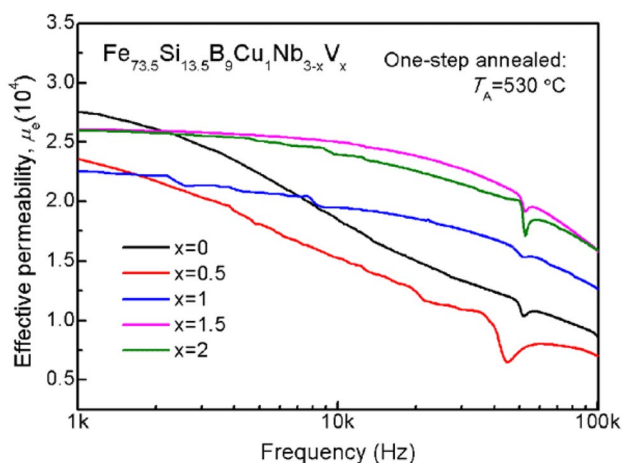

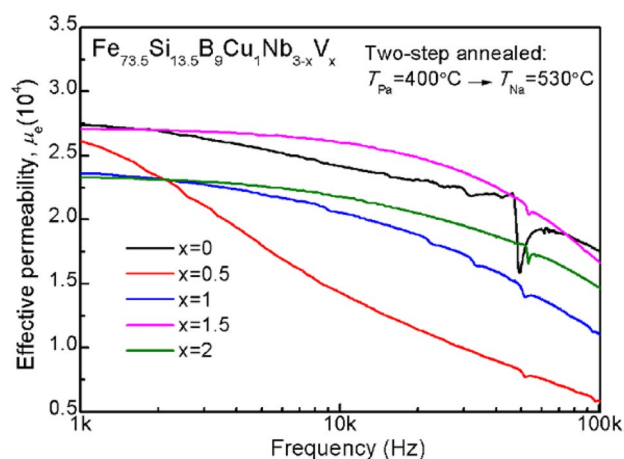**Fig. 5** Effective permeability as a function of applied field frequency for the as-quenched $Fe_{73.5}Si_{13.5}B_9Cu_1Nb_{3-x}V_x$ (x = 0, 0.5, 1, 1.5 and 2) alloys of two-step annealing stage: pretreated at 400 °C for 1h then annealed at 530 °C for 1 h

of x = 0.5 and 1.5 increase to about 27,000. It is clearly observed that except the alloy with V element of x = 0.5, all the other alloys annealed by two-step annealing technique exhibit high stability of μ_e. Especially, the V-free alloy obtained by two-step annealing technique also exhibit a stable μ_e within a wider range of applied field frequency, even at 40 kHz its μ_e still reaches 21,800. Simultaneously, the approach of two-step annealing also promote the increase of cut-off frequency of the alloys.

The core loss is another critical factor for soft magnetic parts and devices, low core loss is required for energy saving and environmental protection. Core loss dependence
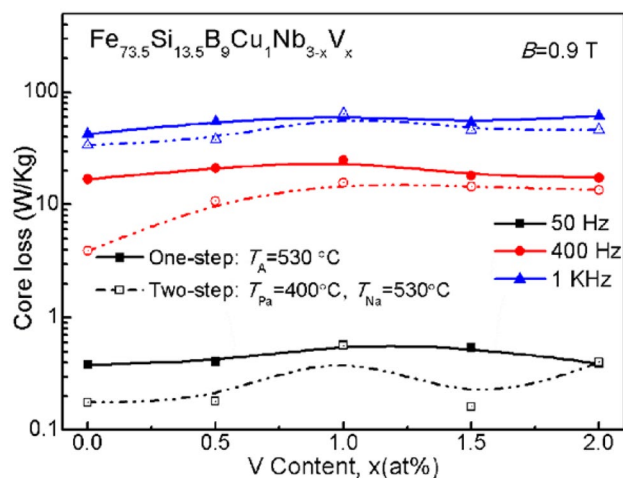

Fig. 4 Effective permeability as a function of applied field frequency for the as-quenched $Fe_{73.5}Si_{13.5}B_9Cu_1Nb_{3-x}V_x$ (x = 0, 0.5, 1, 1.5 and 2) alloy ribbons of one-step annealing at 530 °C for 1h

Fig. 6 Changes of Core loss for the as-quenched $Fe_{73.5}Si_{13.5}B_9Cu_1Nb_{3-x}V_x$ (x = 0, 0.5, 1, 1.5 and 2) ribbons as a function of V content at one-step and two different annealing stages of optimized temperature for 1h

on the frequency for the $Fe_{73.5}Si_{13.5}B_9Cu_1Nb_{3-x}V_x$ ($x = 0$, 0.5, 1, 1.5 and 2) nanocrystalline alloys is shown in Fig. 6. Even applied high magnetic flux density (B_m) of 0.9 T, all of the alloy ribbons still exhibit low core losses. For all the nanocrystalline alloy ribbons, their core losses slightly increase with the initial increase of V content. However, the core losses of the samples prepared with two-step stage are obviously lower than these two-step annealed samples at each composition point of the alloys. As a result, the two-step annealing technique can remediate the unfavorable effect caused by the decrease in noble-metal Nb in the conventional nanocrystalline alloys. Therefore, the lower core loss for the two-step annealing should be attributed to the good soft magnetic properties. Table 1 summarizes hermal parameters and magnetic properties of $Fe_{73.5}Si_{13.5}B_9Cu_1Nb_{3-x}V_x$ ($x = 0$, 0.5, 1, 1.5 and 2) alloys annealed by different technique ,respectively.

To illustrate this experimental situation, we can reasonably correlate the magnetic anisotropy to the structural variations in the presented alloys. The most important contribution to soft magnetic properties is magneto-crystalline anisotropy. In the case that the structural correlation length D is smaller than basic ferromagnetic correlation length L_0 ($\approx 20 \sim 40$ nm for Fe-based alloys), the local randomly oriented anisotropies are averaged by the smoothing effect of exchange interactions, resulting in good soft magnetic properties. From the measured XRD results, as shown in Fig. 7, all peaks can only be indexed to α-Fe phase with a body-centered cubic structure. Meanwhile all the grain size of the α-Fe phase for each annealed sample starting from the amorphous $Fe_{73.5}Si_{13.5}B_9Cu_1Nb_{3-x}V_x$ ($x = 0$ and 1.5) ribbons is determined to be in the range of $D = 10 \sim 20$ nm, which just right falls into the regime where the structural correlation length D is smaller than L_0. The grain size of the a-Fe phase for each annealed sample was estimated according to the Scherer formula. After undergoing a one-step
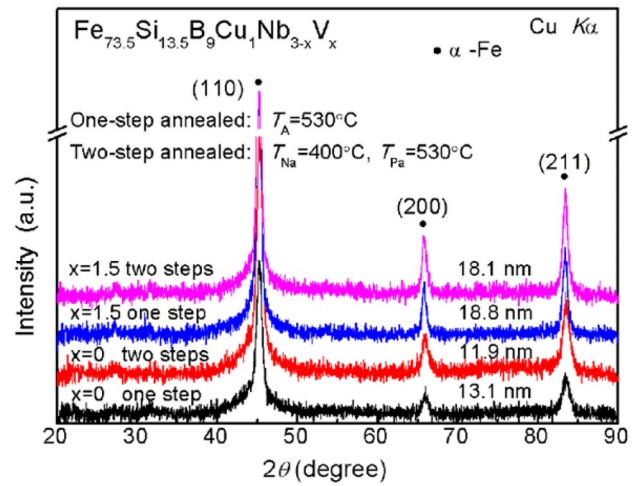

Fig. 7 XRD stages of the $Fe_{73.5}Si_{13.5}B_9Cu_1Nb_{3-x}V_x$ ($x = 0$ and 1.5) alloys prepared after one-step and two-step annealing stage

annealing, the grain size of the α-Fe nanocrystalline phase for the $Fe_{73.5}Si_{13.5}B_9Cu_1Nb_{3-x}V_x$ ($x = 0$ and 1.5) nanocrystalline alloys are 13.1 nm and 18.8 nm, respectively. There appears to be a tendency of increase in the grain size of the nanocrystalline phase along with the V addition. Compared to their counterparts obtained by only one-step, both the two-step annealed $Fe_{73.5}Si_{13.5}B_9Cu_1Nb_{3-x}V_x$ ($x = 0$ and 1.5) alloys possess the crystallization characteristics that their grain size obviously decrease from 13.1 to 11.9 nm and from 18.8 to 18.1 nm, respectively, which is attributed to that preheating at the optimal low temperature of 400 °C promotes the formation of high dense Cu clusters with uniform distribution and thus triggers high nucleation rate. In the regime $D < L_0$, the most significant feature predicted by the random anisotropy model [20] strongly varies with the sixth power of the grain size as $H_c \propto D^6$ and $\mu_e \propto 1/D^6$, which basically explain the improvement in magnetic softness in present work.

Table 1 Thermal parameters and magnetic properties of $Fe_{73.5}Si_{13.5}B_9Cu_1Nb_{3-x}V_x$ ($x = 0$, 0.5, 1, 1.5 and 2) alloys annealed by different technique,respectively

Alloys X (V content)	Thermal parameters ΔT_x(°C)	Annealing technique	Magnetic properties			
			H_c (A/m)	μ_e, (1 kHz)	μ_e, (10 kHz)	B_s (T)
0	130	One step	0.99	27,500	17,600	1.27
		Two step	0.82	27,500	23,000	1.28
0.5	137	One step	1.08	23,500	15,200	1.27
		Two step	0.78	26,000	14,000	1.30
1	145	One step	0.89	22,500	19,000	1.27
		Two step	0.76	23,500	20,500	1.27
1.5	136	One step	1.3	26,100	25,000	1.27
		Two step	0.98	27,000	26,000	1.31
2	126	One step	2.5	26,000	24,000	1.27
		Two step	2.2	23,500	22,000	1.27
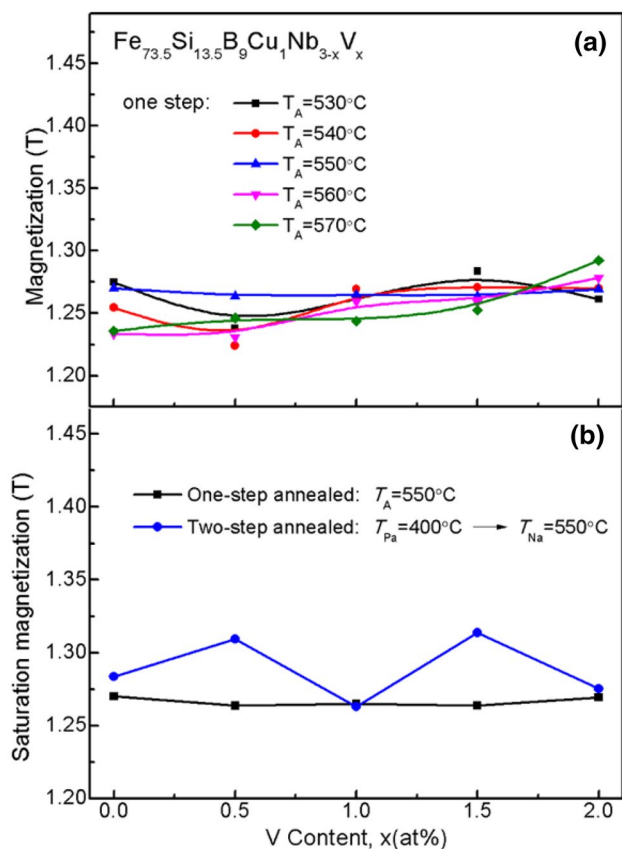
Fig. 8 Changes of B_s for the as-quenched $Fe_{73.5}Si_{13.5}B_9Cu_1Nb_{3-x}V_x$ (x = 0, 0.5, 1, 1.5 and 2) ribbons as a function of V content at one-step annealing (**a**) and two different annealing stages of optimized temperature for 1h (**b**), respectively

Figure 8 indicates the changes of B_s for the $Fe_{73.5}Si_{13.5}B_9Cu_1Nb_{3-x}V_x$ (x = 0, 0.5, 1, 1.5 and 2) nanocrystalline alloys as a function of V content. As shown in Fig. 8a, the values of B_s for the nanocrystalline alloys obtained by one-step annealing show a slight increasing trend with increase V content. The B_s of the $Fe_{73.5}Si_{13.5}B_9Cu_1Nb_3$ alloy at different annealing temperature shows an average value of 1.24 T while the $Fe_{73.5}Si_{13.5}B_9Cu_1Nb_{3-x}V_x$ (x = 0.5, 1, 1.5 and 2) alloys show the average value of 1.25 T, 1.26 T, 1.26 T and 1.27 T, respectively. Furtherly, as shown in Fig. 8b, the two-step annealing technique promotes an obvious increase in B_s at appropriate V content. Commonly, B_s can be expressed by the equation $B_s = RB_{sc} + (1-R)B_{sa}$, where R is the volume fraction of the crystalline phase, B_{sc} and B_{sa} are the saturation magnetization of the crystalline and the amorphous phases, respectively [14]. It is known that B_{sc} (=2.2 T) of the α-Fe phase is almost constant, whereas B_{sa} is relatively small [13]. Therefore, the variation of grain size and volume fraction of the nano-sized α-Fe crystals precipitating from the amorphous matrix is account for the change of B_s.

In order to further determine the effect of V content and pretreatment on the precipitation of α-Fe, crystallization kinetics of the as-quenched and pretreated $Fe_{73.5}Si_{13.5}B_9Cu_1Nb_{3-x}V_x$ (x = 0 and 1.5) amorphous alloys were studied by DSC. Generally, the activation energy of crystallization can be estimated by the Kissinger Eq. [21]del for nanocrystalline soft

$$\ln \left(T^2/\beta \right) = \ln \left(E_a/R \right) - \ln v + E_a/(R/T) \tag{1}$$

where β, E_a, R, v and T are the heating rate, activation energy, gas constant, frequency factor, and specific temperature, respectively. The Kissinger equation is based on the DSC curves at the heating rates of 0.083, 0.167, 0.333, 0.667 and 0.833 °C/s for as-quenched and pretreated at 400 °C specimens as shown in Fig. 9. By plotting ln (T^2/β) versus $1/T$ obtained from linear heating DSC scan, the apparent activation energy of crystallization can thus be calculated from the slopes of the regressive plots as shown in Fig. 10a, the results of which are plotted in Fig. 10b for the activation energy of nucleation (E_x) and the one for growth (E_p) as function of V content, respectively [22–24]. Clearly, E_x decreases upon increase of V content, implying that the nucleation of α-Fe crystallites is much easier with the addition of V in the amorphous matrix as suggested by the decrease of T_{x1} shown in Fig. 2. It can also be seen that E_p decrease with increasing V content. In the present alloy system, the affinities between Nb-Fe and Nb-Cu atoms with the mixing enthalpies −16 and +3 kJ/mol are stronger than those between V-Fe and V-Cu atoms with the mixing enthalpies of −7 and +5 kJ/mol, respectively, which is accord with the result of the decrease in E_x and E_p. Therefore, the addition of V favors the diffusion of Cu atoms to form the aggregation of Cu atom clusters in the initial annealing stage, but slightly weakens the inhibiting effect of Nb on the growth of α-Fe crystals, which is consistent with the results of XRD as shown in Fig. 7.

For obtaining the fine nanocomposite microstructure, two requirements should be satisfied simultaneously [25]. Firstly, there must be a high number density of nucleation sites in the as-quenched alloy. Secondly, the fast growth of nanocrystals during annealing must be suppressed. As shown in Fig. 10 b, E_x decreases and E_p increases when the alloys are pretreated at 400 °C before the crystallization. The decrease in E_x promotes the formation of α-Fe nucleation, which is due to the fact that the pretreating process before crystallization can further enhance the formation of Cu clusters, providing the more nucleation sites for α-Fe nanocrystals. And the increase in E_p suppresses the growth of α-Fe grains. As a result, the strategy of two-step annealing heat treatment further improve magnetic properties and thus effectively retard magnetic properties deteriorated with the addition of V.
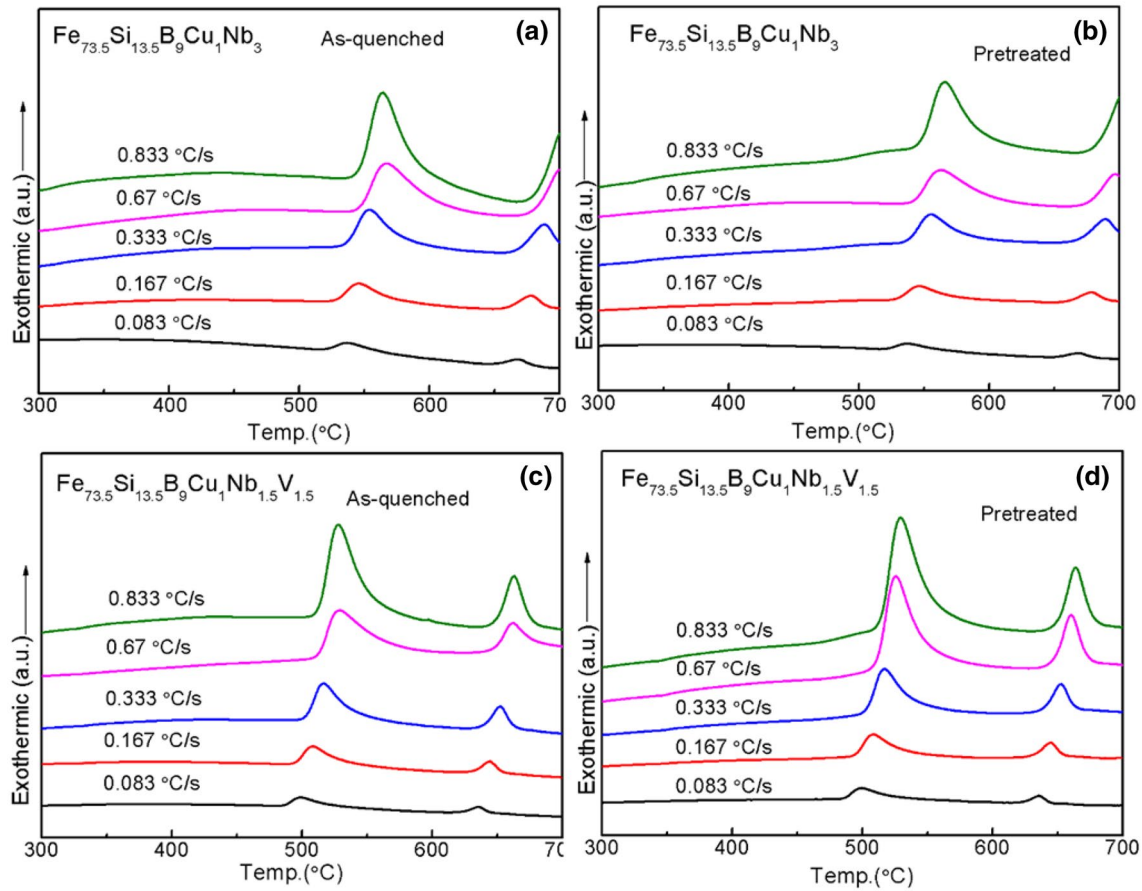
Fig. 9 DSC curves of the as-quenched and pretreated $Fe_{73.5}Si_{13.5}B_9Cu_1Nb_{3-x}V_x$ ($x=0$ and 1.5) amorphous alloys at different heating rate
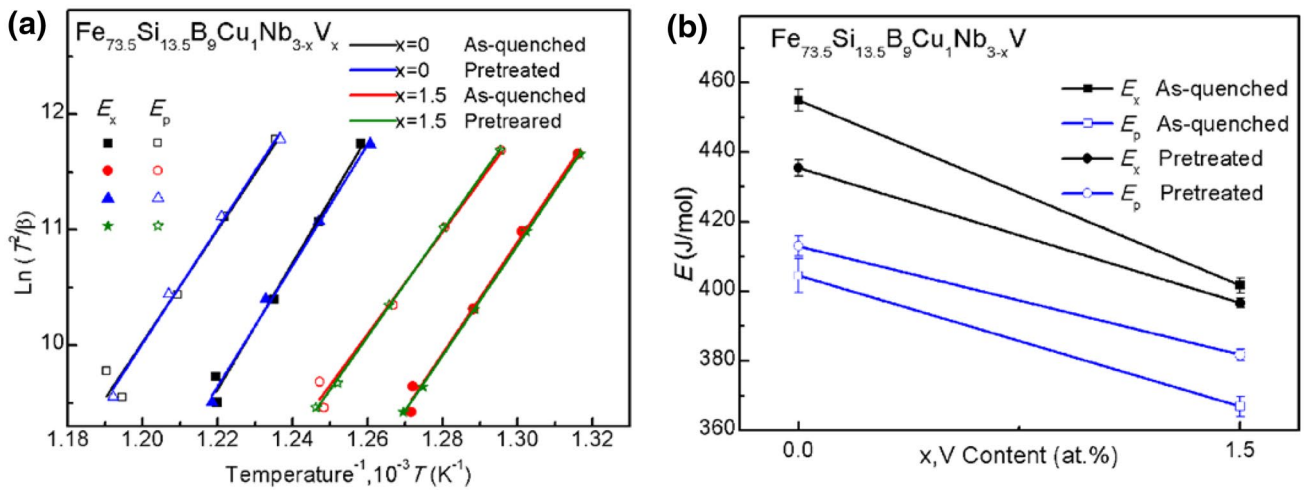

Fig. 10 a Kissinger plots of ln (T^2/β) versus $1/T$ for the as-quenched and pretreated at 400 °C of $Fe_{73.5}Si_{13.5}B_9Cu_1Nb_{3-x}V_x$ ($x=0$ and 1.5) alloys **b** V content dependence of E_x and E_p of $Fe_{73.5}Si_{13.5}B_9Cu_1Nb_{3-x}V_x$ ($x=0$ and 1.5) alloys

For purpose of understanding the effect of V content and two-step annealing on soft magnetic properties, we investigated the magnetic domain structure of the samples prepared with different conditions. Figure 11 shows zero-field magnetic domain patterns observed on the $Fe_{73.5}Si_{13.5}B_9Cu_1Nb_{3-x}V_x$ ($x=0$ and 1.5) ribbons
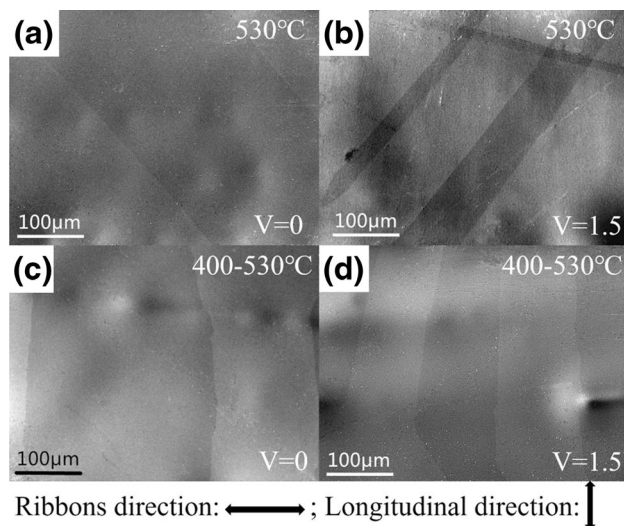
Fig. 11 Zero-field magnetic domain patterns observed on the $Fe_{73.5}Si_{13.5}B_9Cu_1Nb_{3-x}V_x$ (x=0 and 1.5) ribbons surface annealed by one-step for (**a**) x=0 and (**b**) x=1.5, and annealed by two-step for (**c**) x=0 and (**d**) x=1.5, respectively

surface. As shown in Fig. 11a, wide straight domains with 180° walls are visible in the $Fe_{73.5}Si_{13.5}B_9Cu_1Nb_3$ one-step annealing samples. After annealing, the residual stress is released and thus the stress induced magnetic anisotropy is greatly decreased, which gives good explanation for the broad domain structure and the good soft magnetic properties. The domains in Fig. 11b are similar with that in Fig. 11a except a small decrease in the width of domains, slightly reducing the suppression of α-Fe growth. Figure 11c, d are zero-field magnetic domain patterns annealed by one-step at 530 °C for the $Fe_{73.5}Si_{13.5}B_9Cu_1Nb_{3-x}V_x$ alloys with x=0 and 1.5, respectively. However, experienced preheating at 400 °C before the primary nanocrystallization annealing, the domain widths for both the alloys with V content of x=0.5 and 1.5 become larger than their counterparts annealed only by one step, respectively. As shown in Fig. 11c, the easy magnetization directions of both the two-step annealed alloys (x=0 and 1.5) change to an orientation along the longitudinal ribbon [26–29], which implies that the stress-induced magnetic anisotropy is further decreased and thus the improved soft magnetic properties (in Fig. 5). In addition, as shown in Fig. 11d, the widths of the domain for the two-step annealed $Fe_{73.5}Si_{13.5}B_9Cu_1Nb_{1.5}V_{1.5}$ alloy is clearly smaller than that of the two-step annealed $Fe_{73.5}Si_{13.5}B_9Cu_1Nb_3$ alloy, which causes the very high stability of against the increase of frequency and higher cut-off frequency [30]. This are consistent with the best soft magnetic properties (in Fig. 4). As nanoscale α-Fe grains with high-permeability are magnetically coupled by a ferromagnetic amorphous matrix,

and the exchange coupling between the two soft magnetic phases leads to a low magnetic anisotropy [31, 32].

4 Summary

The crystallization behavior, soft magnetic properties and microstructure for $Fe_{73.5}Si_{13.5}B_9Cu_1Nb_{3-x}V_x$ nanocrystalline alloys with the V content ranging from x=0 to x=2 have been systemically studied via two different annealed stages and results are summarized as follows.

1. Adequate addition of V enlarges the temperature interval ΔT_x ($=T_{x2}-T_{x1}$), which favors the precipitation of α-Fe and inhibits the precipitation of other compounds.
2. The optimum soft magnetic properties have been obtained at V=1.5 at%. The $Fe_{73.5}Si_{13.5}B_9Cu_1Nb_{1.5}V_{1.5}$ nanocrystalline alloy shows the lower H_c (0.89 A/m), lower core loss, moderate B_s (1.26 T) and the highest stability of μ_e against the increase of frequency. When the frequency of applied field increases to 10 kHz and even to 25 kHz, the values of μ_e keep high levels of 26,400 and 24,500.
3. Two-step annealing technique can further optimize soft magnetic properties by grain refinement as compared with one-step annealing. Through two-step annealing technique, the values of μ_e and B_s for the $Fe_{73.5}Si_{13.5}B_9Cu_1Nb_{1.5}V_{1.5}$ (x=1.5) nanocrystalline alloy greatly increase to about 27,000 and 1.3 T, while H_c and core loss obviously decrease, respectively.

References

1. Y. Yoshizawa, S. Oguma, K. Yamauchi, New Fe-based soft magnetic alloys composed of ultrafine grain structure. J. Appl. Phys. **64**, 6044–6046 (1988)
2. M.A. Willard, D.E. Laughlin, M.E. Mchenry, D. Thoma et al., Structure and magnetic properties of $(Fe_{0.5}Co_{0.5})_{88}Zr_7B_4Cu_1$ nanocrystalline alloys. J. Appl. Phys. **84**, 6773–6777 (1999)
3. M.M. Raja, K. Chattopadhyay, B. Majumdar, A. Narayanasamy, Structure and soft magnetic properties of finemet alloys. J. Alloy Compd. **297**, 199–205 (2000)
4. A. Urata, H. Matsumoto, S. Yoshida, A. Makino, Fe–B–P–Cu nanocrystalline soft magnetic alloys with high Bs. J. Alloy Compd. **509**, S431–S433 (2011)
5. T. Kubota, A. Makino, A. Inoue, Low core loss of $Fe_{85}Si_2B_8P_4Cu_1$ nanocrystalline alloys with high Bs and B800. J. Alloy Compd. **509**, S416–S419 (2011)
6. F.G. Chen, Y.G. Wang, X.F. Miao, H. Hong et al., Nanocrystalline $Fe_{83}P_{16}Cu_1$ soft magnetic alloy produced by crystallization of its amorphous precursor. J. Alloy Compd. **549**, 26–29 (2013)

Ribbons direction: ⟷ ; Longitudinal direction: ↕

7. M.E. Mchenry, M.A. Willard, D.E. Laughlin, Amorphous and nanocrystalline materials for applications as soft magnets. Prog. Mater. Sci. **44**, 291–433 (1999)

8. M.E. McHenry, D.E. Laughlin, Nano-scale materials development for future magnetic applications. Acta. Mater. **48**, 223–238 (2000)

9. M. Ohta, Y. Yoshizawa, High Bs nanocrystalline $Fe_{84-x-y}Cu_xNb_ySi_4B_{12}$ alloys (x = 0.0–1.4, y = 0.0–2.5). J. Magn. Magn. Mater. **321**, 2220–2224 (2009)

10. G. Herzer Grain structure and magnetism of nanocrystalline ferromagnets. IEEE Trans. Magn. 25:3327–3329 (1989)

11. Y. Yoshizawa, Magnetic properties and applications of nano-structured soft magnetic materials. Scr. Mater. **44**, 1321–1325 (2001)

12. M. Ohta, Y. Yoshizawa, New high-Bs Fe-based nanocrystalline soft magnetic alloys. Jpn. J. Appl. Phys. **46**, L477–L479 (2007)

13. M. Ohta, Y. Yoshizawa, Magnetic properties of nanocrystalline $Fe_{82.65}Cu_{1.35}Si_xB1_{6-x}$ alloys (x = 0–7). Appl. Phys. Lett. **91**, 062517 (2007)

14. M. Ohta, Y. Yoshizawa (2007) Improvement of soft magnetic properties in $(Fe_{0.85}B_{0.15})_{100-x}Cu_x$ melt-spun alloys. Mater. Trans. **48**, 2378–2380

15. K. Hono, Atom probe microanalysis and nanoscale microstructures in metallic materials. Acta. Mater. **47**, 3127–3145 (1999)

16. K. Hono, D.H. Ping, M. Ohnuma, H. Onodera, Cu clustering and Si partitioning in the early crystallization stage of an $Fe_{73.5}Si_{13.5}B_9Nb_3Cu_1$ amorphous alloy. Acta. Mater. **47**, 997–1006 (1999)

17. T. Bitoh, A. Makino, A. Inoue, (2004) The effect of grain-size distribution on coercivity in nanocrystalline soft magnetic alloys. J. Magn. Magn. Mater. **272–276**(2) 1445–1446

18. T. Bitoh, A. Makino, A. Inoue, T. Masumoto, Random anisotropy model for nanocrystalline soft magnetic alloys with grain-size distribution. Mater. Trans. **44**, 2011–2019 (2003)

19. Y. Han, A. Wang, A. He, C. Chang et al., Improvement of magnetic properties, microstructure and magnetic structure of $Fe_{73.5}Cu_1Nb_3Si_{15.5}B_7$ nanocrystalline alloys by two-step annealing process. J. Mater. Sci. **27**, 1–6 (2016)

20. G. Herzer, Modern soft magnets: Amorphous and nanocrystalline materials. Acta. Mater. **61**, 718–734 (2013)

21. H.E. Kissinger, Reaction kinetics in differential thermal analysis. Anal. Chem. **29**, 1702–1706 (1957)

22. S.H. Al-Heniti, Kinetic study of non-isothermal crystallization in $Fe_{78}Si_9B_{13}$ metallic glass. J. Alloy Compd. **484**, 177–184 (2009)

23. D.M. Minić, A. Gavrilović, P. Angerer, D.G. Minić et al., Thermal stability and crystallization of $Fe_{89.8}Ni_{1.5}Si_{5.2}B_3C_{0.5}$ amorphous alloy. J. Alloy Compd. **482**, 502–507 (2009)

24. X.F. Miao, Y.G. Wang, M. Guo, Structural, thermal and magnetic properties of Fe–Si–B–P–Cu melt-spun ribbons: Application of non-isothermal kinetics and the amorphous random anisotropy model. J. Alloy Compd. **509**, 2789–2792 (2011)

25. A. Inoue, Stabilization of metallic supercooled liquid and bulk amorphous alloys. Acta. Mater. **48**, 279–306 (2000)

26. R. Schäfer, Domains in 'extremely' soft magnetic materials. J. Magn. Magn. Mater. **215–216**:652–663 (2000)

27. K. Suzuki, N. Ito, S. Saranu, U. Herr et al., Magnetic domains and annealing-induced magnetic anisotropy in nanocrystalline soft magnetic materials. J. Appl. Phys. **103**, 07E730–07E733 (2008)

28. L. Kraus, K. Závěta, O. Heczko, P. Duhaj, et al., Magnetic anisotropy in as-quenched and stress-annealed amorphous and nanocrystalline $Fe_{73.5}Cu_1Nb_3Si_{13.5}B_9$ alloys. J. Magn. Magn. Mater. **112**, 275–277 (1992)

29. S. Flohrer, R. Schäfer, C. Polak, G. Herzer, Interplay of uniform and random anisotropy in nanocrystalline soft magnetic alloys. Acta. Mater. **53**, 2937–2942 (2005)

30. R. Schafer, A. Hubert, G. Herzer, Domain observation on nanocrystalline material. J. Appl. Phys. **69**, 5325–5327 (1991)

31. S. Flohrer, R. Schäfer, J. McCord, S. Roth et al., Magnetization loss and domain refinement in nanocrystalline tape wound cores. Acta. Mater. **54**, 3253–3259 (2006)

32. S. Flohrer, R. Schäfer, G. Herzer, Magnetic microstructure of nanocrystalline FeCuNbSiB soft magnets. J. Non-Cryst. Solids **354**, 5097–5100 (2008)